Red-Emitting Polymerizable Guanidinium Dyes as Fluorescent Probes in Molecularly Imprinted Polymers for Glyphosate Detection

Martha Kimani,† Víctor Pérez-Padilla,† Virginia Valderrey, Kornelia Gawlitza and Knut Rurack*

Chemical and Optical Sensing Division, Bundesanstalt für Materialforschung und-prüfung (BAM), Richard-Willstätter Straße 11, 12489 Berlin, Germany; martha-wamaitha.kimani@bam.de (M.K.); victor.perez-padilla@bam.de (V.P.-P.); virginia.valderrey-berciano@bam.de (V.V.); kornelia.gawlitza@bam.de (K.G.)

* Correspondence: knut.rurack@bam.de

† These authors contributed equally to this work.

Table of Contents:

1. NMR spectra of 2-((7-(3-benzoylguanidino)benzo[c][1,2,5]oxadiazol-4-yl)-(methyl)amino)ethyl methacrylate

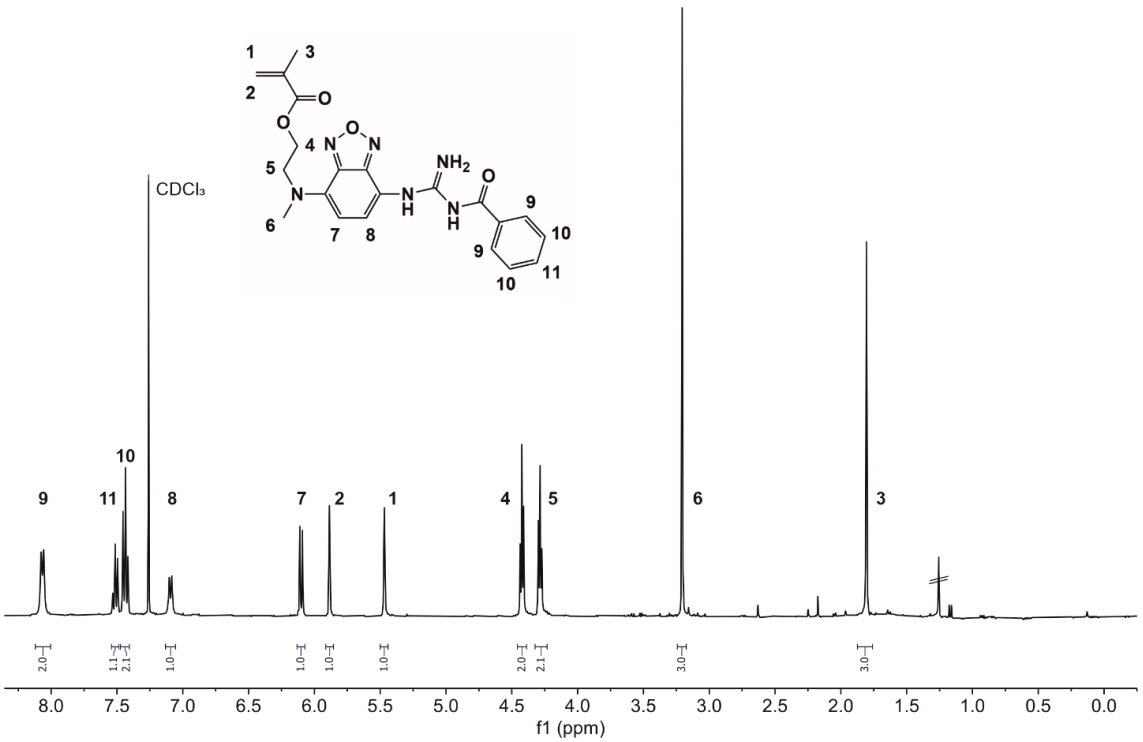

Figure S1. ^{1}H-NMR (400 MHz, $CDCl_3$) spectrum of 2-((7-(3-benzoylguanidino)benzo[c][1,2,5]oxadiazol-4-yl)(methyl)amino)ethyl methacrylate.

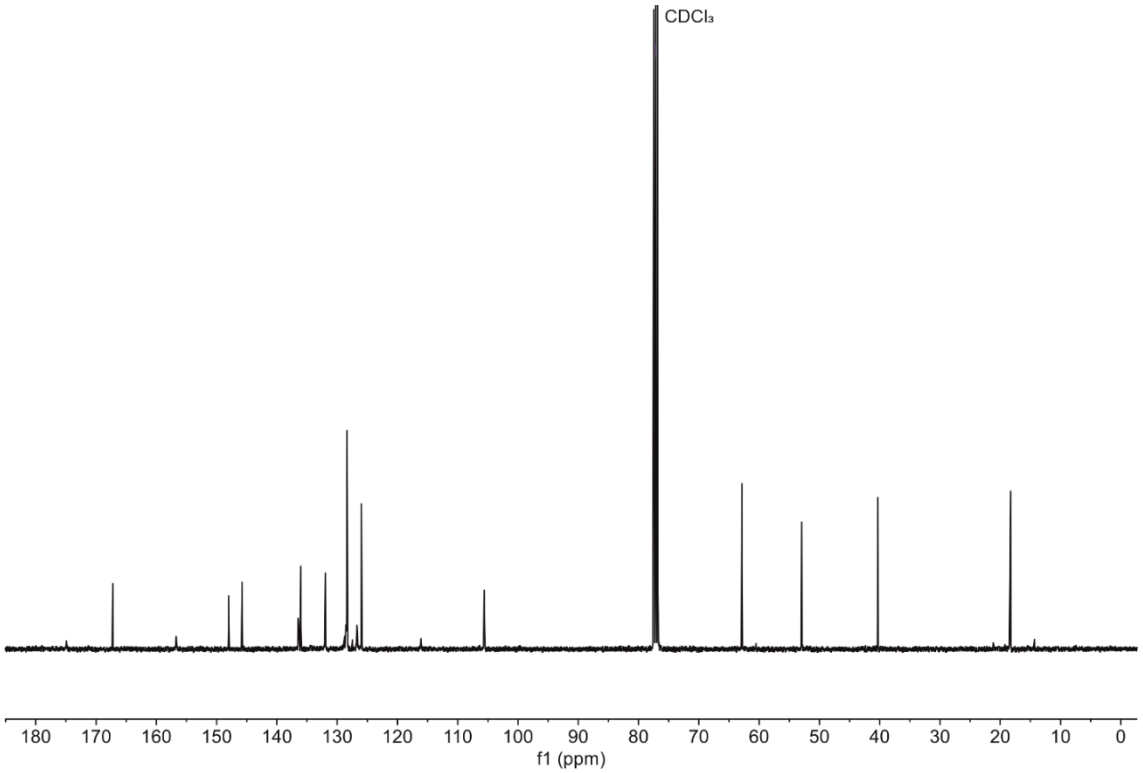

Figure S2. ^{13}C-NMR (100 MHz, $CDCl_3$) spectrum of 2-((7-(3-benzoylguanidino)benzo[c][1,2,5]oxadiazol-4-yl)(methyl)amino)ethyl methacrylate.

2. NMR spectra of fluorescent monomer I

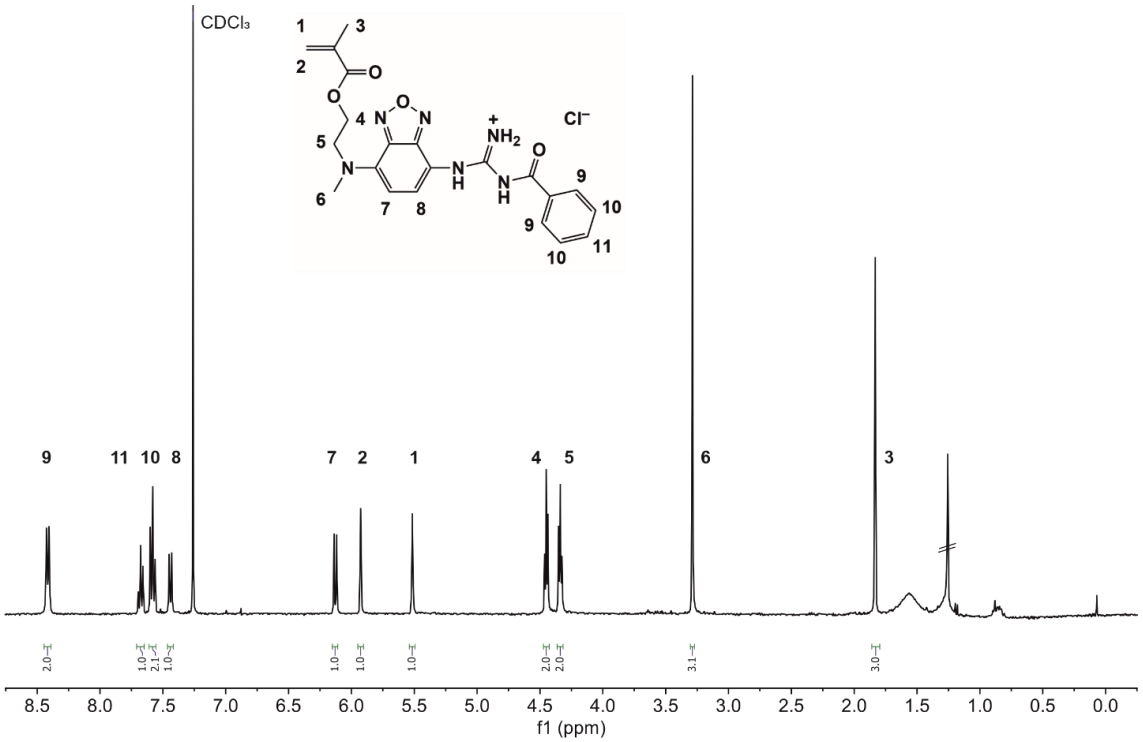

Figure S3. ^{1}H-NMR (400 MHz, $CDCl_3$) spectrum of compound **I**.

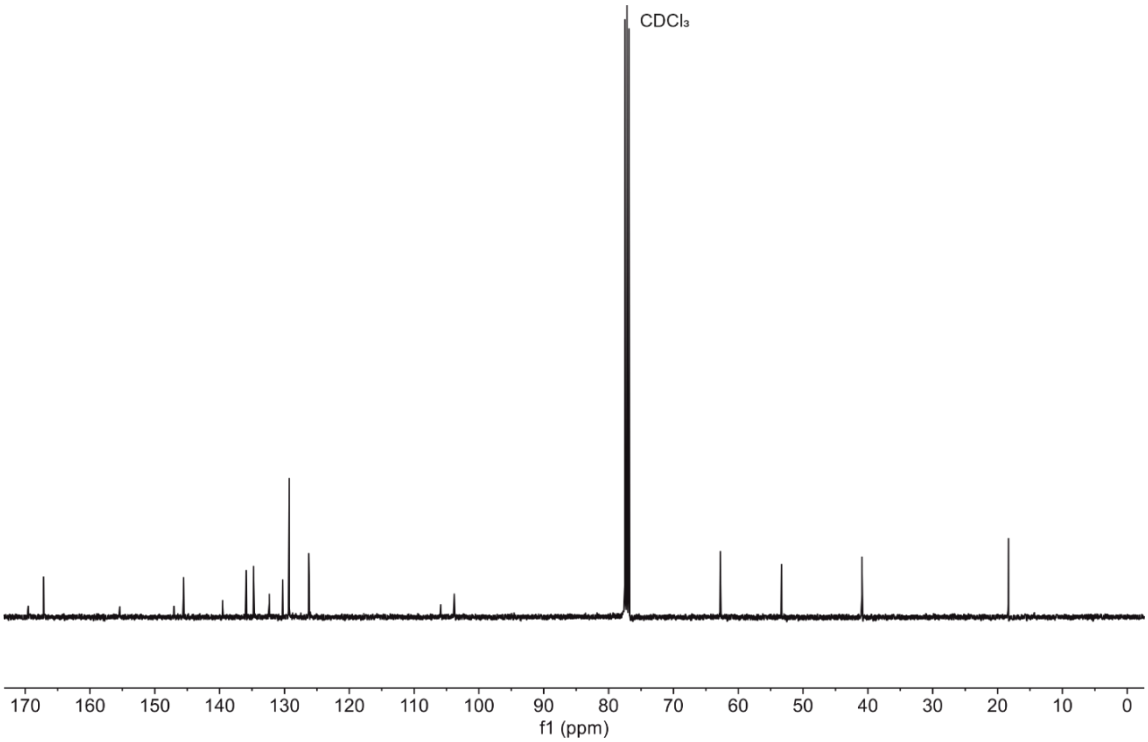

Figure S4. ^{13}C-NMR (100 MHz, $CDCl_3$) spectrum of compound **I**.

3. Mass spectra of fluorescent compounds

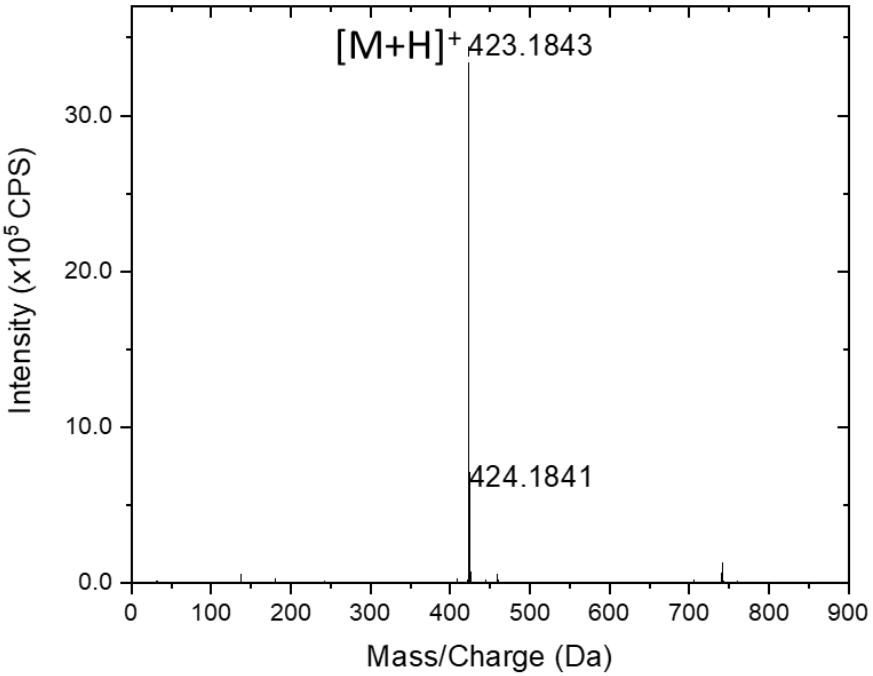

Figure S5. HRMS spectrum of 2-((7-(3-benzoylguanidino)benzo[c][1,2,5]oxadiazol-4-yl)(methyl)amino)ethyl methacrylate. The molecular peak corresponds to the base peak at m/z = 423.1843.

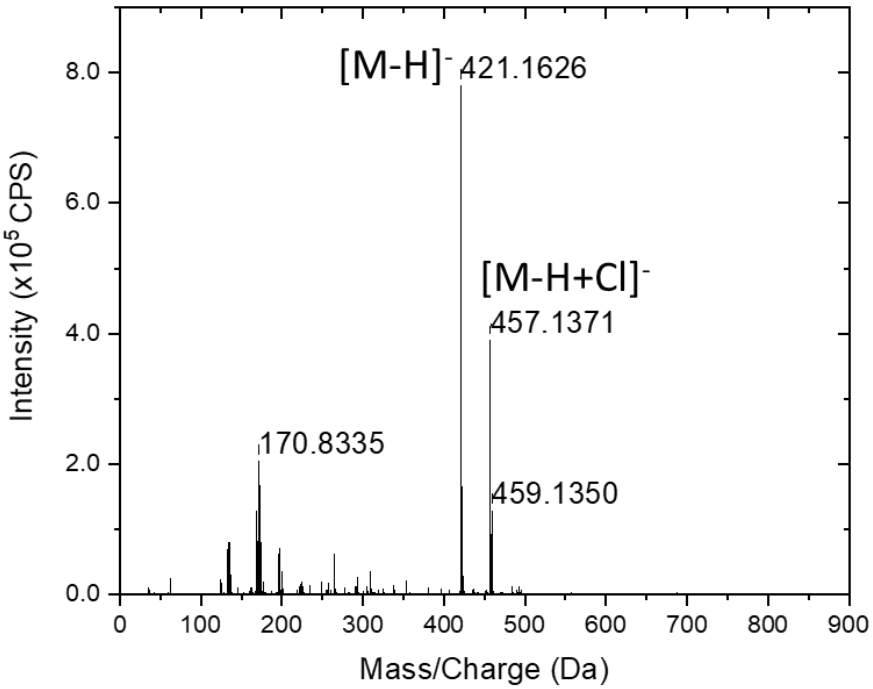

Figure S6. HRMS spectrum of compound **I**. The molecular peak is at m/z = 457.1371.

4. Synthesis of silica particles

Silica particles were synthesized according to the Stöber method, with modifications [1]. First, 65 mL of 96% ethanol, 121 mL of Milli-Q water and 14 mL of 32% ammonia solution were mixed at 300 rpm in a 1 L Erlenmeyer flask. Then, 18 mL of TEOS (80 mmol) was mixed with 182 mL of 96% ethanol and quickly added to the base solution. The mixture was stirred overnight at 300 rpm. The resulting particles were washed thrice with 96% ethanol by centrifugation and redispersion at 12,700× *g* for 10 min, then dried overnight in a vacuum.

5. Modification of silica particles with APTES

APTES modification of silica particles was performed as previously reported [1]. First, 1 g of silica particles was weighed into a two-necked round bottomed flask equipped with a magnetic stirrer and connected to a reflux condenser. The particles were dispersed in 50 mL of anhydrous toluene and heated to 120 °C under argon. Then, 4 mL of APTES (17.1 mmol) was added and the reaction was allowed to proceed for 16 h under reflux. The particles were then washed thrice with 35 mL of 96% ethanol, with centrifugation at 12,700× *g* for 5 min and with 5 min sonication between washes. The particles (**APTES@SiO$_2$**) were dried overnight in a vacuum.

6. Modification of APTES@SiO$_2$ particles with reversible-addition fragmentation chain transfer (RAFT) agent

Modification of the **APTES@SiO$_2$** particles for reversible-addition fragmentation chain transfer (RAFT) polymerization was performed according to previously published protocols [1]. Briefly, 500 mg of **APTES@SiO$_2$** particles were weighed into a 20 mL vial equipped with a magnetic stirrer and placed in an ice bath. Simultaneously, 117.4 mg of the RAFT agent CPDB (0.4 mmol), 40.3 µL of ethyl chloroformate (0.4 mmol) and 58.7 µL of triethylamine (0.4 mmol) were dissolved in 8.6 mL of anhydrous tetrahydrofuran (THF) and mixed together in an acetone/liquid nitrogen bath at –78 °C for 40 min. Afterwards, the cooled solution was added to the particles and left to react at room temperature for 24 h at 700 rpm. The particles were precipitated with 15 mL of n-hexane and centrifugation performed at 12,700× *g* for 5 min. The particles were washed once with 20 mL of THF, once with 20 mL of acetone and in 20 mL of THF once more, with centrifugation at 12,700× *g* for 5 min and with 5 min sonication between washes. The particles (**RAFT@SiO$_2$**) were then dried in a vacuum overnight.

7. Absorption and emission of compound I in CHCl$_3$ and MeCN

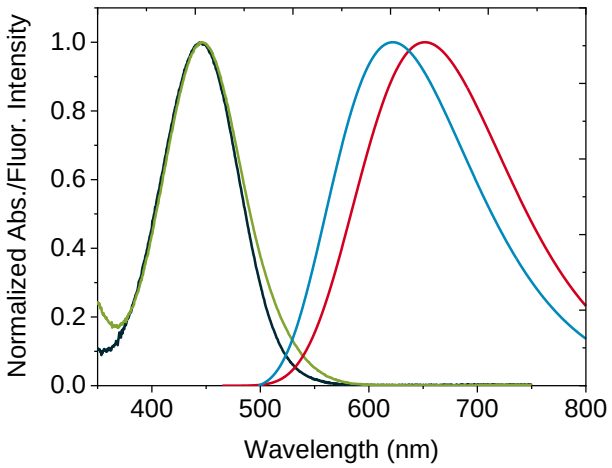

Figure S7. Normalized absorption and fluorescence emission spectra (λ_{ex} = 445 nm) of compound **I** (c[**I**] = 1 x 10^{-5} M) in MeCN and $CHCl_3$. The black and the red curves are the absorption and the emission in MeCN, respectively; while the green and the blue curves are the absorption and the emission in $CHCl_3$, respectively.

8. Excitation spectra of compound I upon addition of GPS-TBA in $CHCl_3$ and MeCN

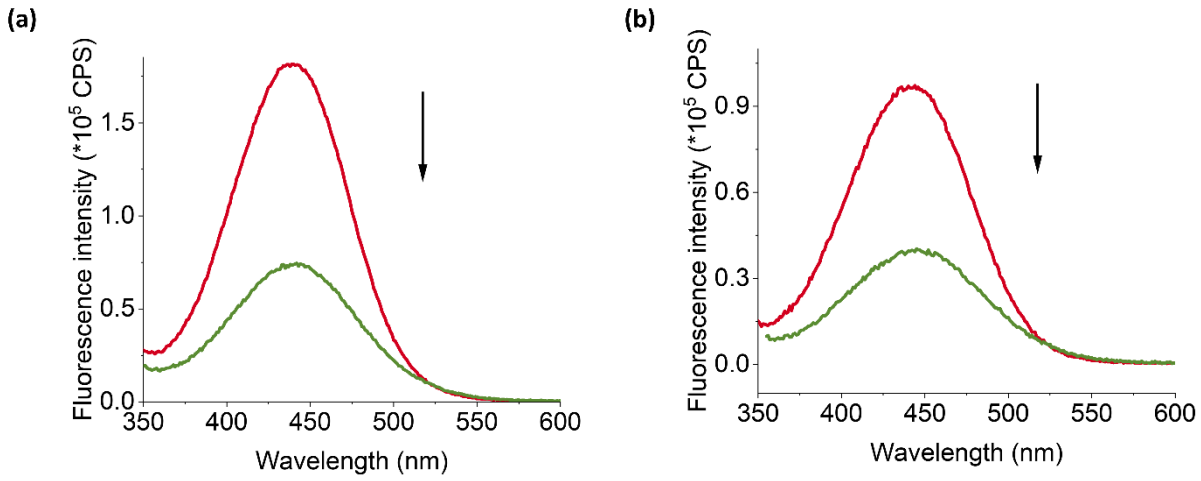

Figure S8. (**a**) Excitation spectra of **I** (6.5 μM, λ_{em} = 622 nm, red line) upon addition of 1.4 equivalents of GPS-TBA (9.2 μM, λ_{em} = 650 nm, green line) in $CHCl_3$. (**b**) Excitation spectra of **I** (6.5 μM, λ_{em} = 652 nm, red line) upon addition of 1.5 equivalents of GPS-TBA (9.9 μM, λ_{em} = 680 nm, green line) in MeCN.

9. Determination of binding constants of I with templates

All titrations were performed at 22 ± 2°C. Association constants were determined by the non-linear fitting of absorption data using BindFit, a free online tool accessible at http://app.supramolecular.org/bindfit/, accessed between 03.06.–29.10.2020 [2]. The algorithm used assumes that the guest (template) is non-absorbing and non-fluorescent, and that dynamic quenching does not occur, which all apply to the systems studied.

10. Job plot (method of continuous variation) for interaction of I with GPS-TBA in $CHCl_3$ and MeCN

The Job plots were constructed as previously reported [3]. For a continuous variations diagram, the difference Y_λ between the measured absorbance A_λ and the calculated absorbance A_λ' is plotted against the molar fraction x of one reactant (in this case GPS-TBA). The absorbances measured for the pure solutions of GPS-TBA (subscript M) and **I** (subscript L) are used to calculate A_λ', according to Equation S1. In the experiment, solutions of different molar ratios are prepared from equimolar solutions of M and L and the actual absorbance A_λ is measured. Then, Y_λ is calculated (Equation S2) and, when plotting Y_λ vs. x_M, maxima at x_M = 0.5, 0.33 and 0.25 are found for 1:1, 1:2 and 1:3 (M:L) complexes, respectively. GPS-TBA does not possess an absorption signal.

$$A_\lambda' = x_M \varepsilon(\lambda)_M c_M d + x_L \varepsilon(\lambda)_L c_L d$$ Equation S1

$$Y_\lambda = A_\lambda - A_\lambda'$$ Equation S2

with $c_{M0} = c_{L0}$ and $x_M + x_L = 1$.

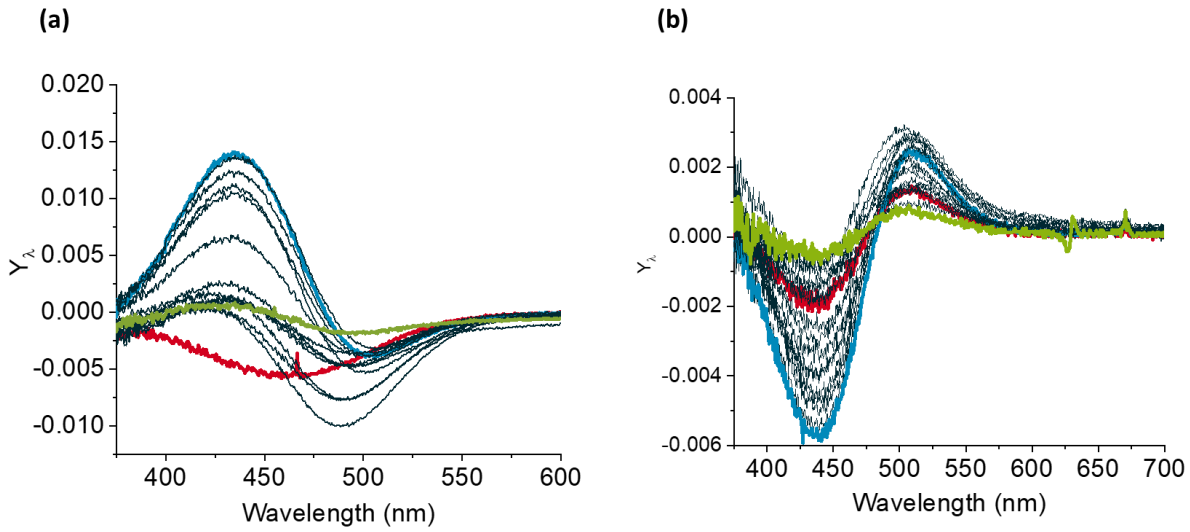

Figure S9. (**a**) Y_λ for the different molar ratios for **I** and GPS-TBA in $CHCl_3$. Red line represents 90% of **I**, blue line 60% of **I** and green line 10% of **I**. The binding is consistent with 1.5:1 (L:M) stoichiometry (**b**) Y_λ for the different molar ratios for **I** and GPS TBA in MeCN. The red line represents 90% of **I**, the blue line represents 63% of **I** and the green line, 10% of **I**. The binding is consistent with 2:1 (L:M) stoichiometry.

11. ^{1}H NMR titrations of compound I with GPS-TBA in CD_3CN

To better understand the results of the spectroscopic titrations in acetonitrile with an independent method, ^{1}H NMR titrations were carried out in CD_3CN. The fluorescent monomer **I** was used at 5×10^{-3} M and was added to the template salt solution at the same concentration prior to the titration. For comparison, the ^{1}H NMR spectrum of GPS-TBA (Figure S10) in CD_3CN is shown in Figure S11, and Figure S12 recollects the ^{1}H NMR spectrum of compound **I** in CD_3CN.

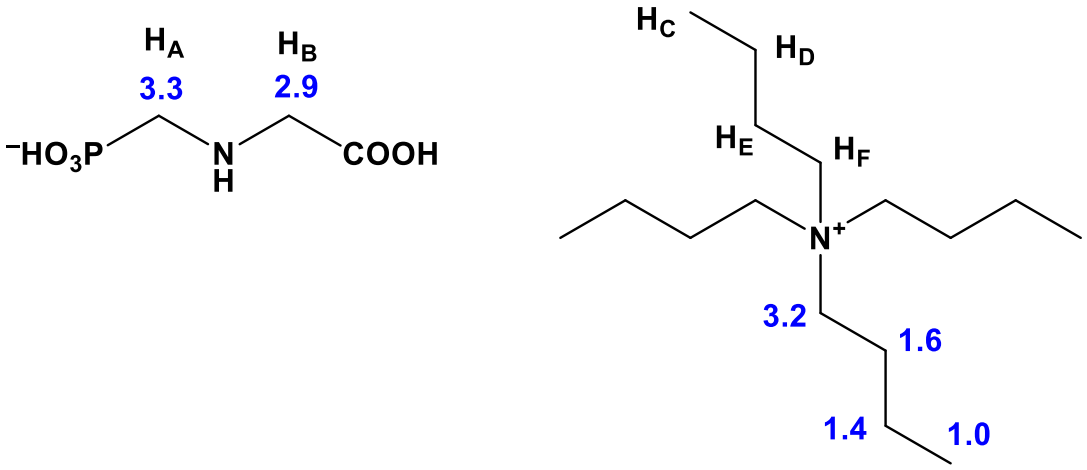

Figure S10. Numbering of the assignable protons of GPS-TBA for NMR analysis and their predicted chemical shifts (realized with ChemDraw).

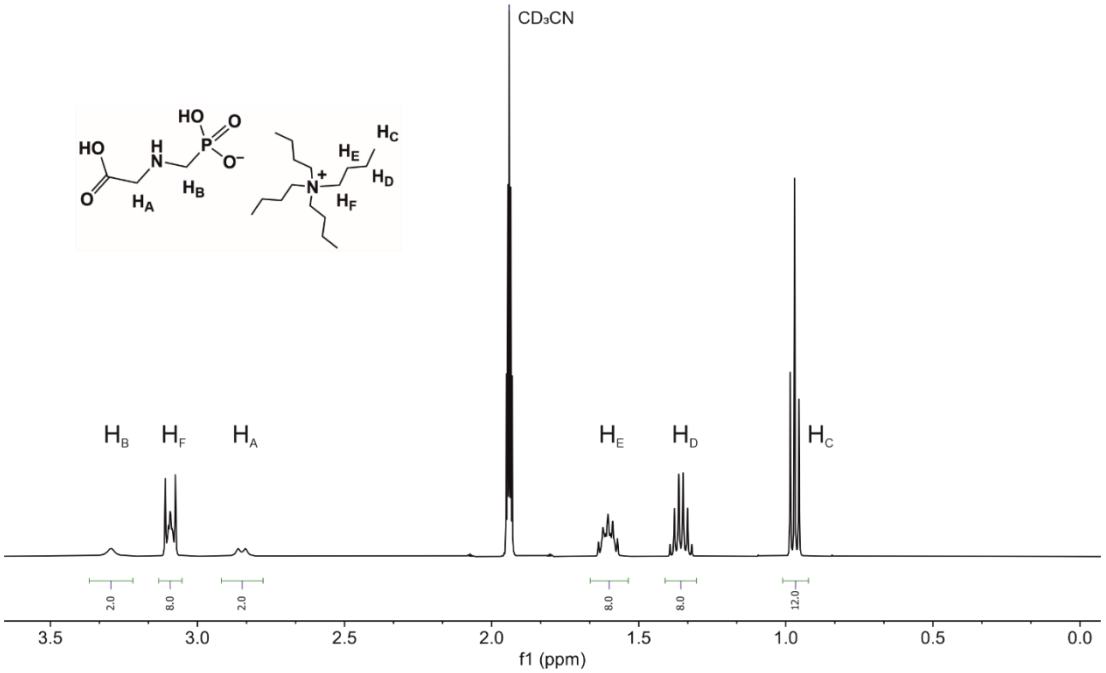

Figure S11. ^{1}H-NMR spectrum of GPS-TBA in CD_3CN prepared in an equimolar amount. The ratio of GPS to TBA is calculated 1.0 to 1.0. ^{1}H-NMR (500 MHz, CD_3CN): δ (ppm) = 3.29 (s, 2H), 3.09 (m, 8H), 2.85 (d, 2H), 1.60 (m, 8H), 1.36 (sext, 8H), 0.97 (t, 12H).

The 12 methyl protons H_C of the TBA cation appear at 0.97 ppm, and the 3 × 8 protons of the methylene groups (H_D–H_F) of the four butyl chains progressively appear at 1.36, 1.60 and 3.09 ppm, with decreasing distances to the ammonium nitrogen. The two methylene protons between the NH and the COOH groups (H_B) of GPS appear at 2.85 ppm, and the two methylene protons between the NH and the PO_3H^- groups (H_A) are found at 3.29 ppm. The NH, COOH and PO_3H^- could not be clearly distinguished in the spectra.

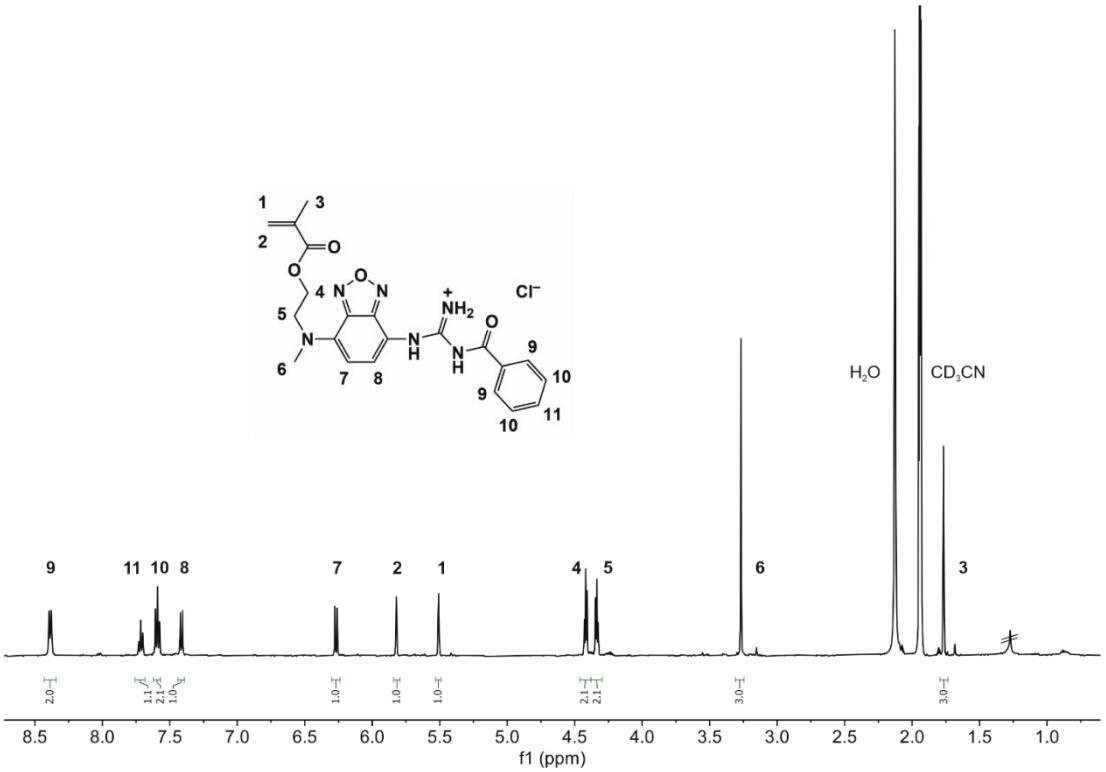

Figure S12. ^{1}H-NMR (500 MHz, CD_3CN) spectrum of compound **I**.

Figures S13 and S14 show the titration spectra of compound **I** with increasing amounts of GPS-TBA, while Figures S15 and S16 show the titration spectra of GPS-TBA with increasing amounts of compound **I**, namely, the reverse titration. Figures S14 and S16 zoom into the relevant regions where pronounced shifts are observable.

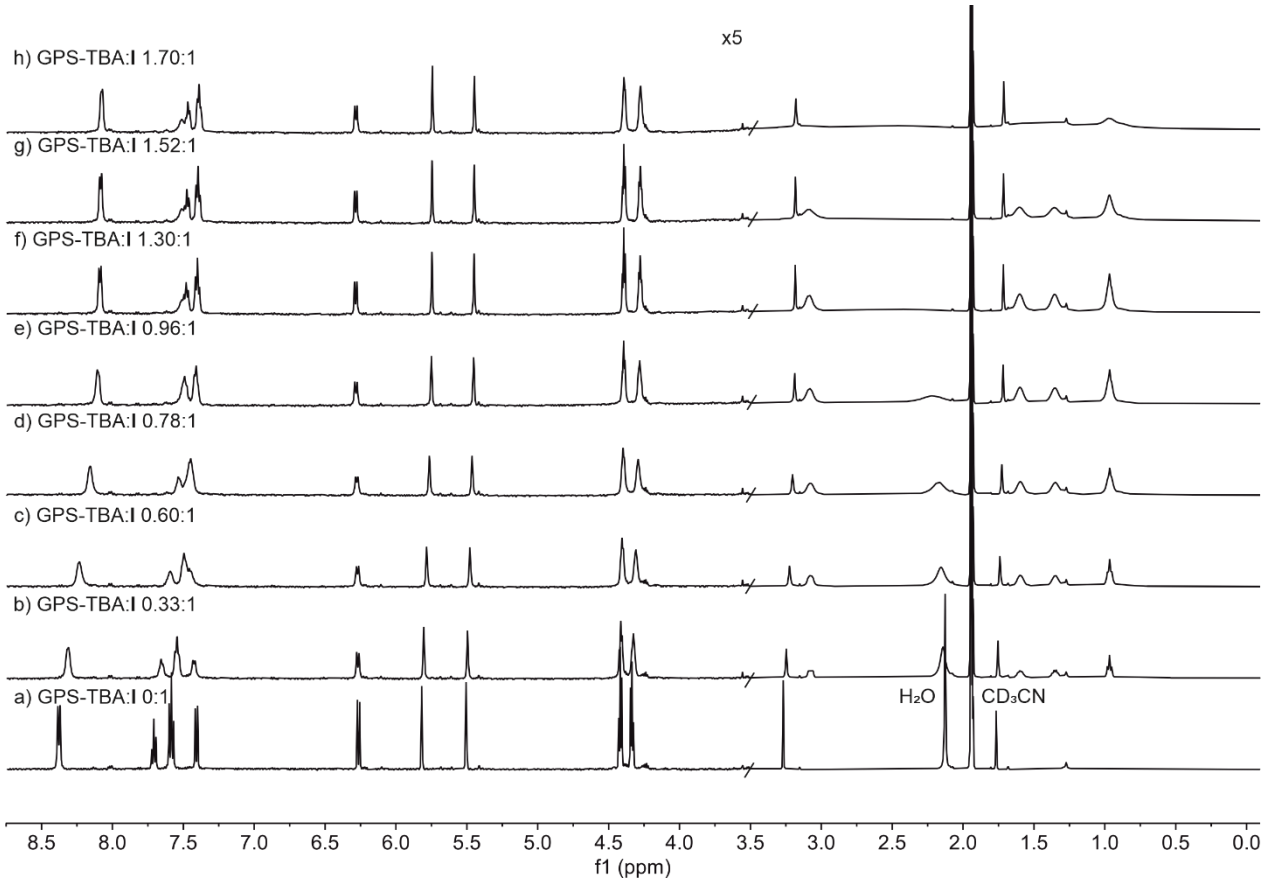

Figure S13. ^{1}H NMR (500 MHz, CD_3CN) titration spectra of **I** with GPS-TBA. The equivalents of GPS-TBA that are present in the different steps are (from bottom to top): 0.00, 0.33, 0.60, 0.78, 0.96, 1.30, 1.52, 1.70. The equivalents are experimentally calculated by the relation of the integral of the proton signal H_C of GPS-TBA to the integral of the proton signal H_5 of compound **I** (Figures S11, S12). The concentration of the dye is constant along the titration ($c_I = 5 \times 10^{-3}$ M).

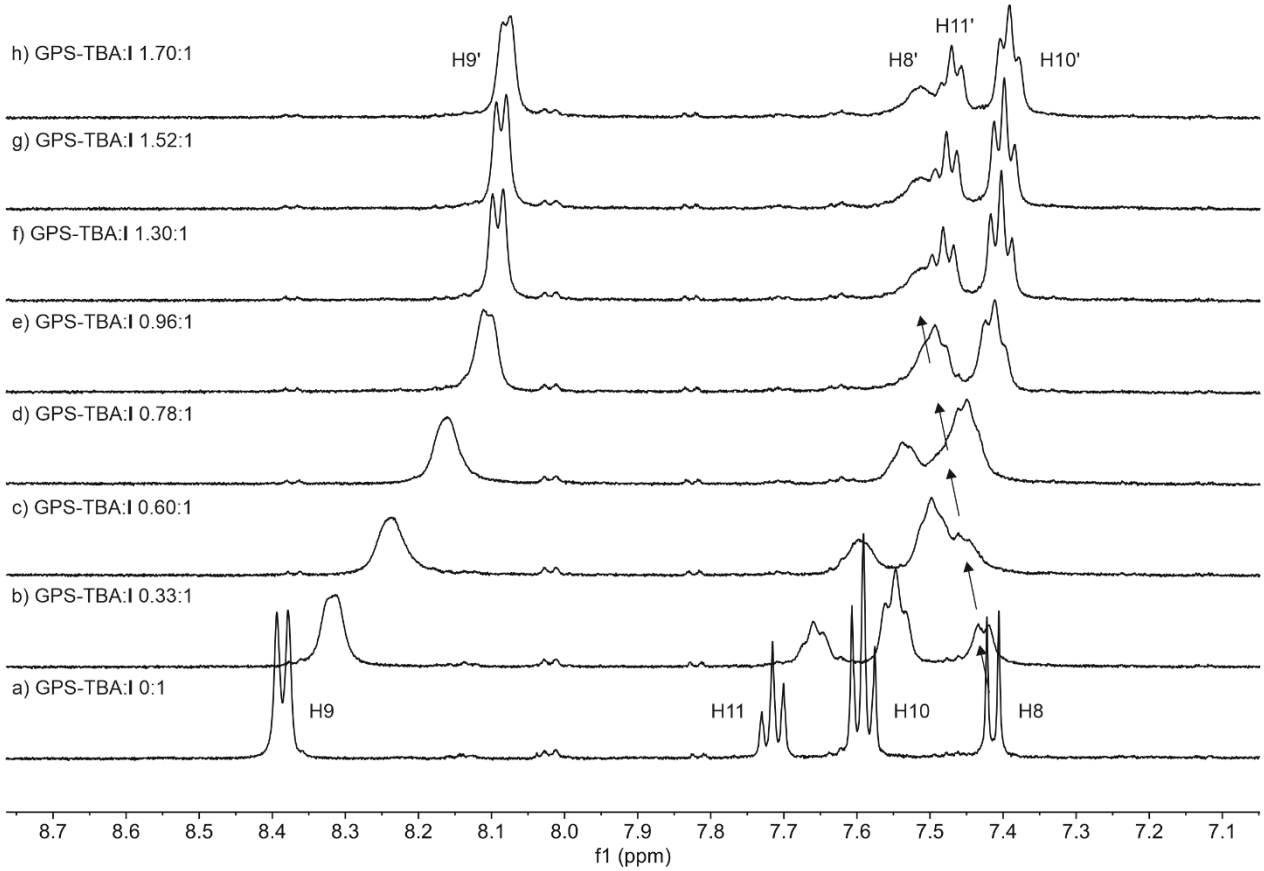

Figure S14. Magnification of the aromatic region of the ^{1}H NMR (500 MHz, CD_3CN) titration spectra of **I** with GPS-TBA shown in Figure S13. The equivalents of GPS-TBA present in the different steps are (from bottom to top): 0.00, 0.33, 0.60, 0.78, 0.96, 1.30, 1.52, 1.70; $c_I = 5 \times 10^{-3}$ M. Inverted commas denote the proton signals of complexed compound **I**.

The most significant shifts in the titration in CD_3CN are the upfield shifts of H9, H11 and H10 to positions H9′, H11′ and H10′ in the complex as well as the downfield shift of H8 to H8′ in the aromatic region. Signal H9 was selected as the reference, which shifted from 8.39 ppm to 8.10 ppm. The shifts of the aromatic signals H9, H11 and H10 follow the expected trend for the hydrogen bonding of GPS-TBA to **I**. The binding of GPS-TBA to **I** injects electron density into the aromatic system, resulting in a de-shielding and upfield shift of the proton signals of compound **I**.

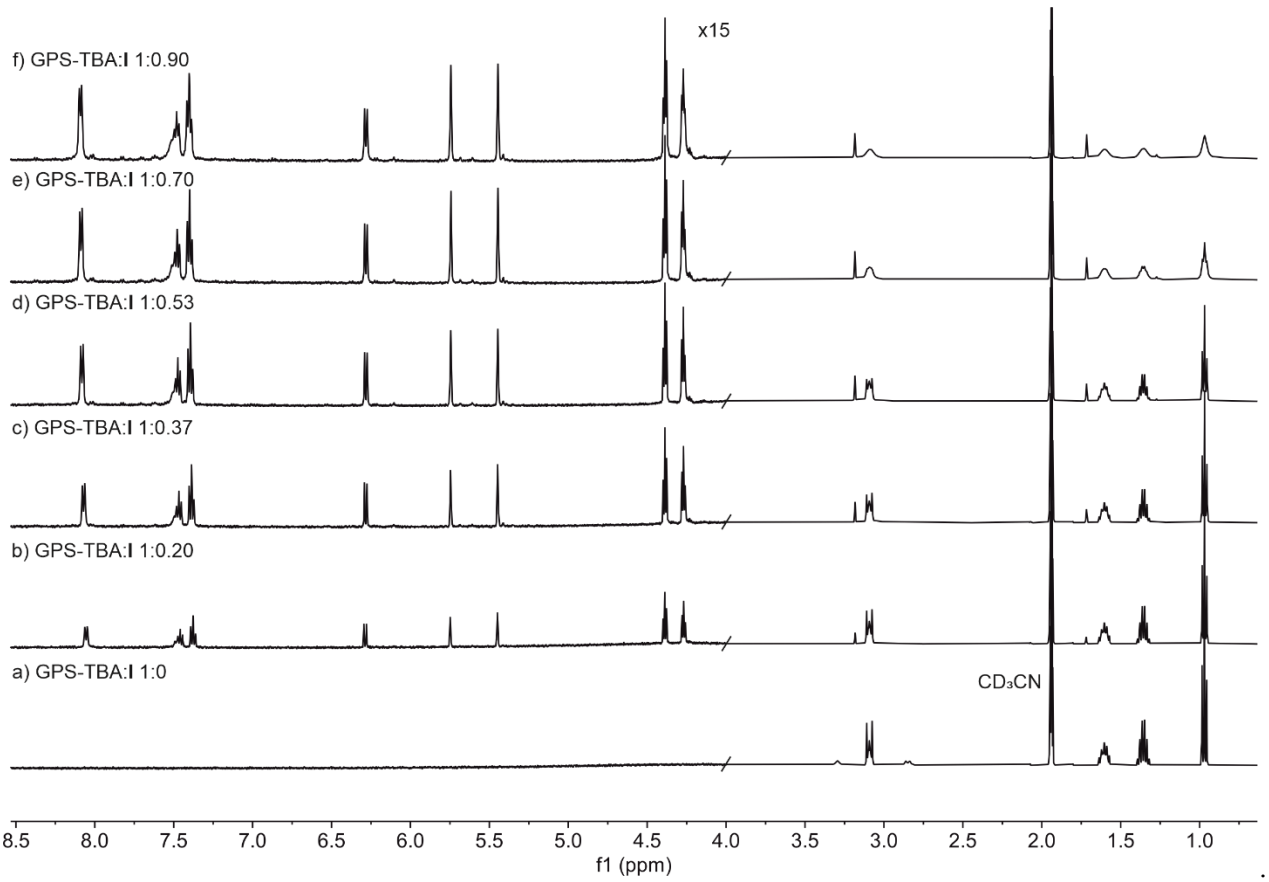

Figure S15. ^{1}H NMR (500 MHz, CD_3CN) titration spectra of GPS-TBA with **I**. The equivalents of compound **I** present in the different steps are (from bottom to top): 0.00, 0.20, 0.37, 0.53, 0.70 and 0.90. The equivalents are experimentally calculated by the relation of the integral of the proton signal H_5 of compound **I** to the integral of the proton signal H_C of GPS-TBA (Figures S11, S12). The concentration of GPS-TBA is constant along the titration ($c_{GPS\text{-}TBA} = 5 \times 10^{-3}$ M).

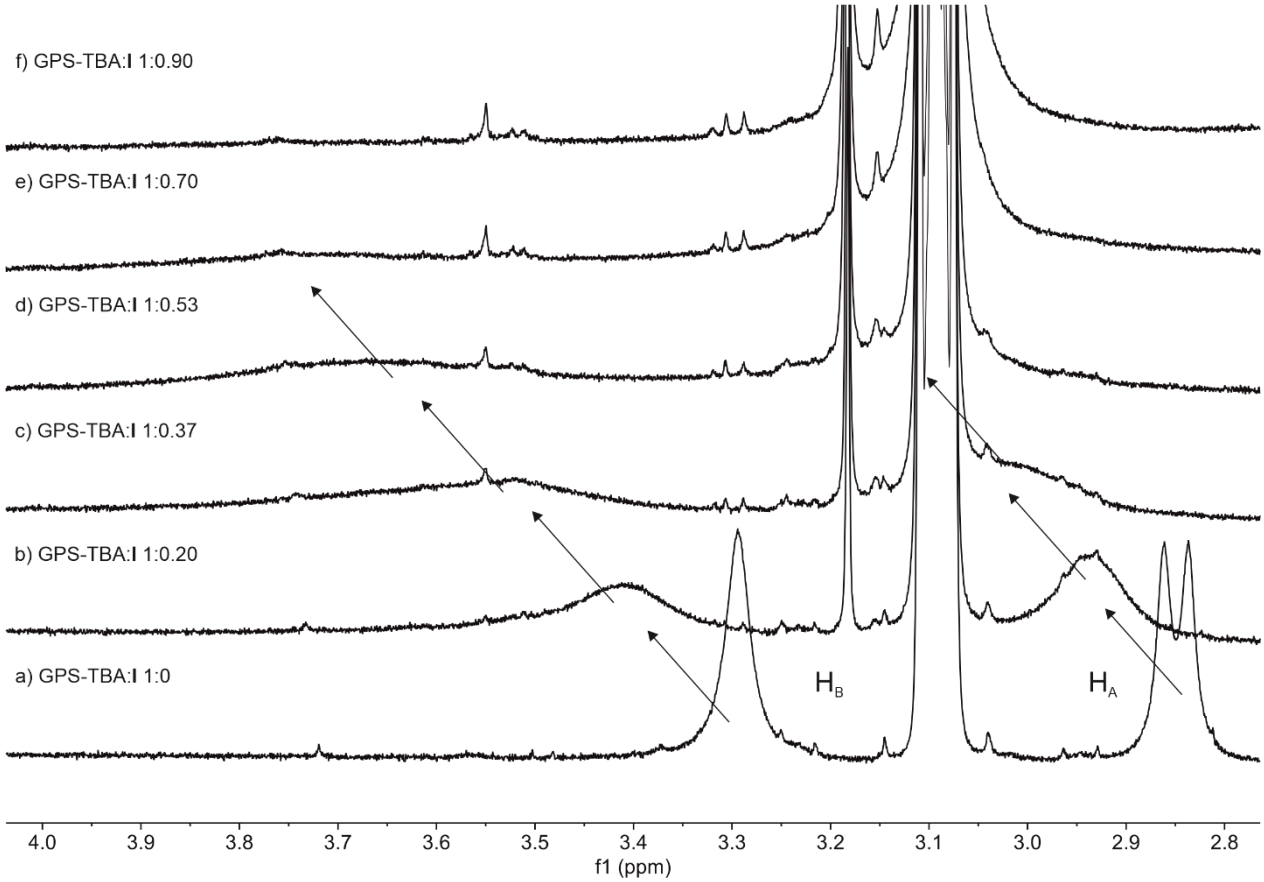

Figure S16. Magnification of the GPS region of the ^{1}H NMR (500 MHz, CD_3CN) titration spectra of GPS-TBA with **I**. The equivalents of compound **I** present in the different steps are (from bottom to top): 0.00, 0.20, 0.37, 0.53, 0.70 and 0.90; $c_{GPS\text{-}TBA} = 5 \times 10^{-3}$ M.

Because the proton signals of GPS could not be detected in the titration of compound **I** with GPS-TBA in CD_3CN, a reverse titration of GPS-TBA with compound **I** was carried out (Figures S15, S16). Here, it was observed that both GPS proton signals H_A and H_B experience a downfield shift and extensive broadening until the signals are no longer detectable, in accordance with the previous titrations. The downfield shifts can be explained by the shielding of the GPS signals as a result of the donation of electron density, through hydrogen bonding from GPS to compound **I**. The shift of the GPS proton signal H_A can be followed up to 0.37 equivalents of **I**; past this point, the signal overlaps with the TBA proton signal H_F. The GPS proton signal H_B can be detected up to 0.70 equivalents of **I**. When higher amounts of compound **I** are added, the proton signal H_B is too broad to be reliably detected. Moreover, in the reverse titration, the proton signal H9' of compound **I,** for instance, is always found at 8.10 ppm, matching the position of proton H9' at the endpoint when compound **I** is titrated with GPS-TBA (see Figures S13, S14).

In conclusion, the NMR measurements in CD_3CN reveal a clear 1:1 binding mode at millimolar concentrations and support the spectroscopic findings, at micromolar concentrations, that a 2:1 complex is only a very minor species.

12. Zeta potential measurements

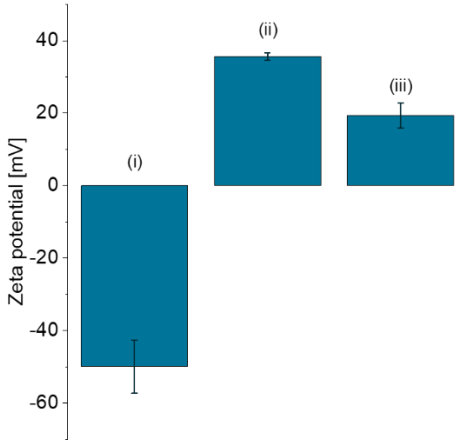

Figure S17. Zeta potential measured at pH 6 of (i) SiO_2 particles, (ii) **APTES@SiO$_2$**, (iii) **RAFT@SiO$_2$**.

13. Determination of surface area of silica core particles with the Brunauer-Emmett-Teller (BET) theory

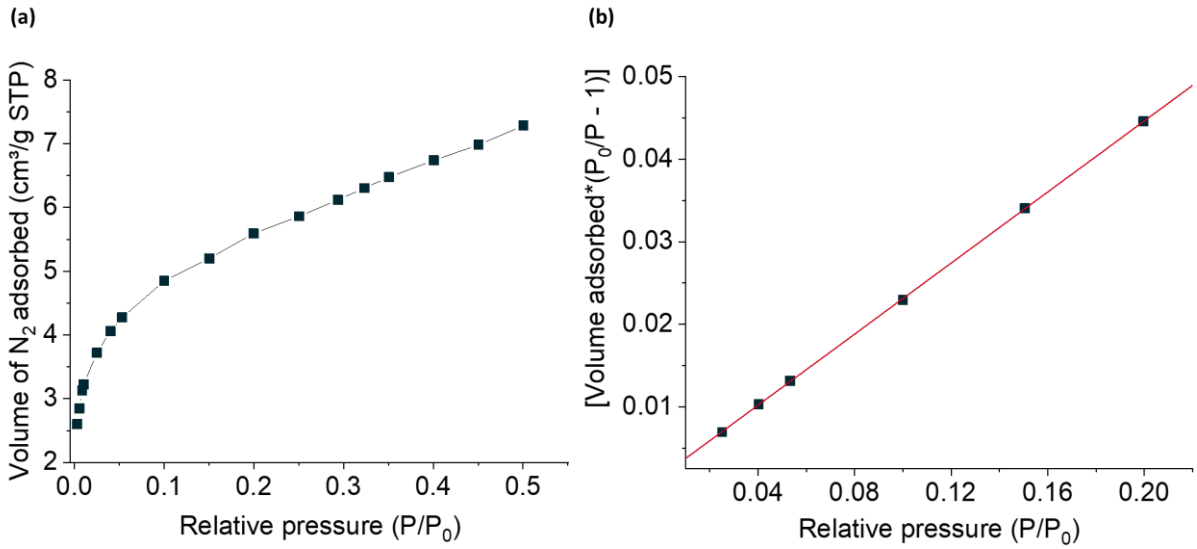

Figure S18. (**a**) Volume of nitrogen adsorbed per gram of SiO_2 and (**b**) BET surface area plot.

14. Interaction of MPA-TBA with compound I in $CHCl_3$ and MeCN

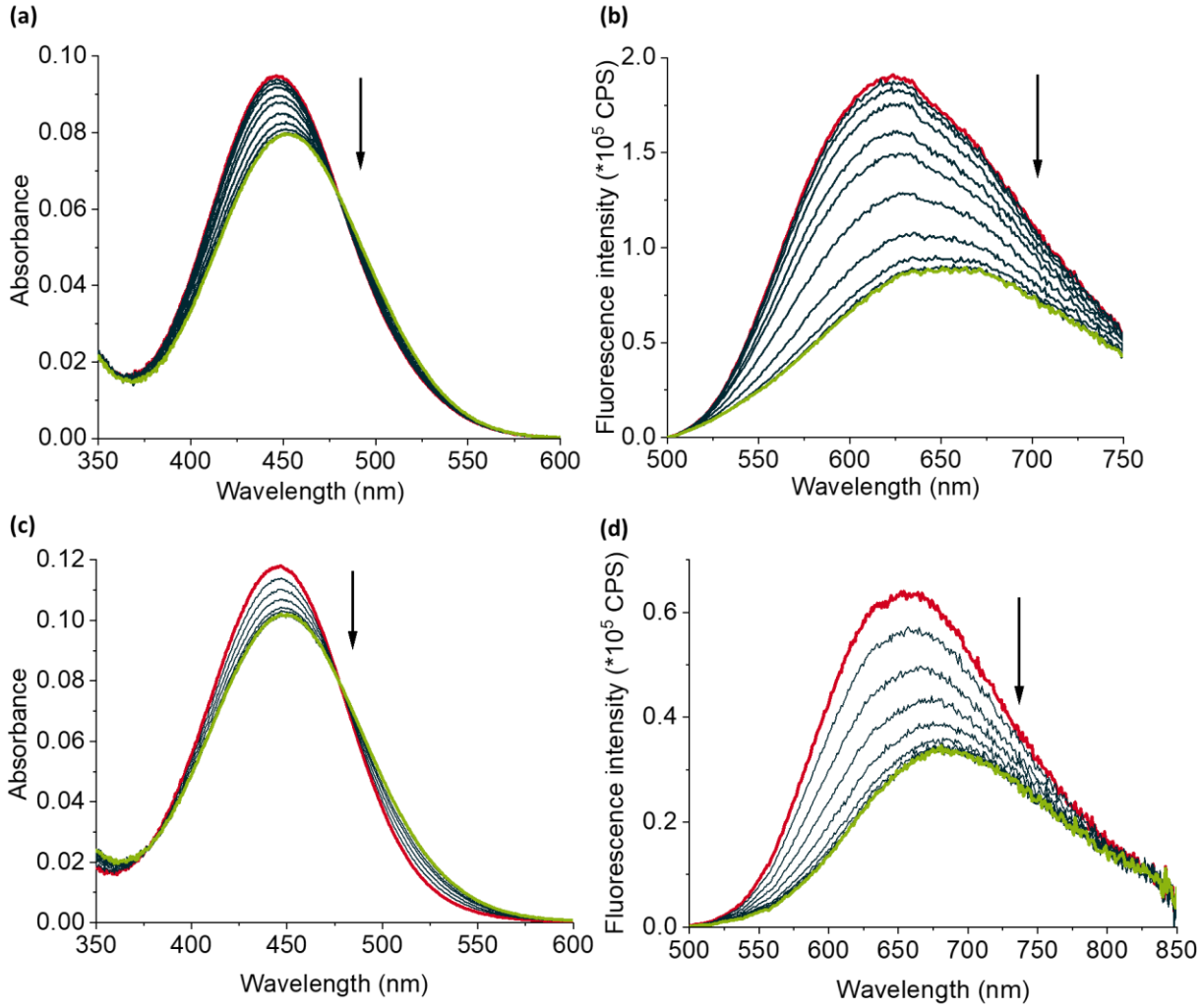

Figure S19. (**a**) Absorption and (**b**) fluorescence spectra (λ_{ex} = 474 nm) for titration of **I** (10.8 μM) with MPA-TBA (0.4–37.2 μM) in $CHCl_3$. Red line is spectrum of **I** in $CHCl_3$, while the green line shows the spectrum of **I** after addition of up to 3.4 equivalents of MPA-TBA. The binding fit a 1:1 stoichiometry, with $K^{CHCl_3}_{I\text{-}MPA\text{-}TBA}$ = 3.18 (±0.03) × 10^5 M^{-1}. (**c**) Absorption and (**d**) fluorescence spectra (λ_{ex} = 479 nm) for titration of **I** (10.0 μM) with MPA-TBA (2.0–19.8 μM) in MeCN. The red line is the spectrum of **I** in MeCN, while the green line shows the spectrum of **I** after addition of up to 2.0 equivalents of MPA-TBA. The binding fits a 1:1 stoichiometry, with $K^{MeCN}_{I\text{-}MPA\text{-}TBA}$ = 1.18 (±0.07) × 10^7 M^{-1}.

15. Absorption spectra of pre-polymerization mixtures for MIP and dNIP synthesis

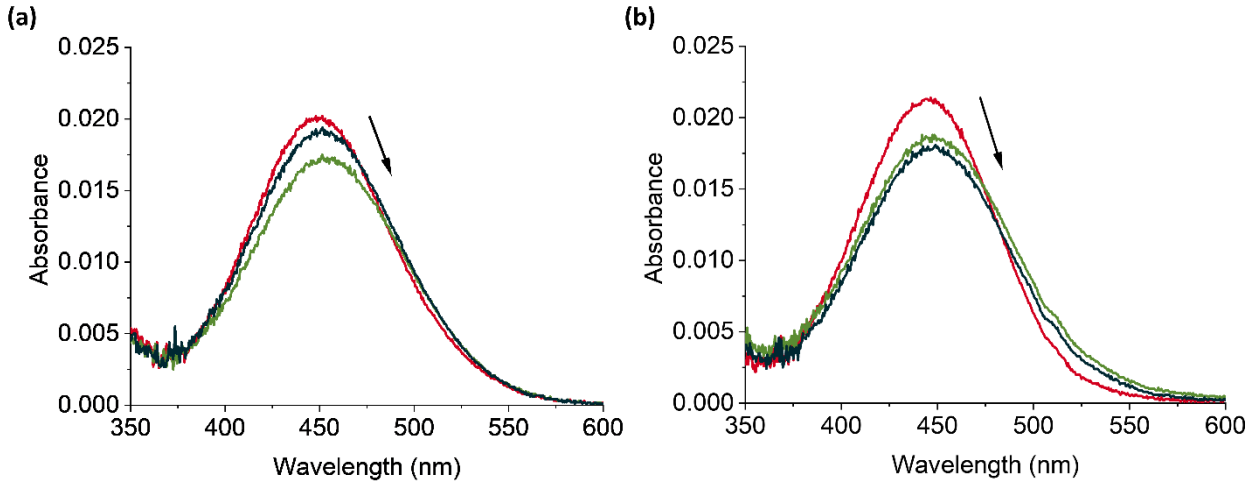

Figure S20. Absorption spectra of pre-polymerization mixtures of the different MIP and dNIP particles, using a 1:1 stoichiometry of **I**:GPS-TBA or **I**:MPA-TBA. (**a**) Spectra in $CHCl_3$ of **I** + MAAm + EGDMA (red line), **I** + MAAm + EGDMA + GPS-TBA (green line) and **I** + MAAm + EGDMA + MPA-TBA (black line). Equimolar amounts of **I** and GPS-TBA and **I** and MPA-TBA were used. (**b**) Spectra in MeCN of **I** + MAAm + EGDMA (red line), **I** + MAAm + EGDMA + GPS-TBA (green line) and **I** + MAAm + EGDMA + MPA-TBA (black line).

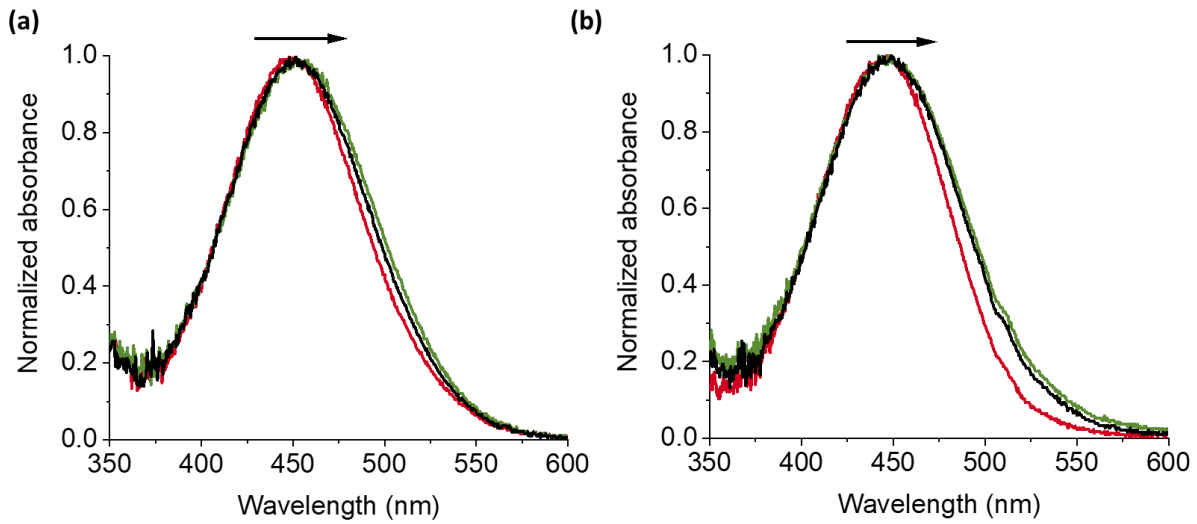

Figure S21. Normalized absorption spectra of pre-polymerization mixtures of the MIP and dNIP particles using a 1:1 stoichiometry of **I**:GPS-TBA or **I**:MPA-TBA. (**a**) Spectra in $CHCl_3$ of **I** + MAAm + EGDMA (red line), **I** + MAAm + EGDMA + GPS-TBA (green line) and **I** + MAAm + EGDMA + MPA-TBA (black line). (**b**) Spectra in MeCN of **I** + MAAm + EGDMA (red line), **I** + MAAm + EGDMA + GPS-TBA (green line) and **I** + MAAm + EGDMA + MPA-TBA (black line).

16. Determination of the amount of dye incorporated into MIP and dNIP particles

Following MIP synthesis, significant shifts in the wavelength of maximum absorption **I** in MIP and dNIP particles were observed, compared to the diluted solution. Consequently, the molar absorption coefficient of the dye at the wavelength of maximum absorption could not be used to accurately determine the concentration of incorporated dye in the MIP and dNIP particles. Instead, the area under the absorption curve of a known concentration of **I** in the respective solvents ($CHCl_3$ or MeCN) was used as a comparison for its determination. The absorption spectra of stock solutions of the dye were recorded with three replicates in a quartz cuvette with 1 cm optical path length. The absorption spectra of known particle concentrations of the MIP and dNIP particles were recorded in MeCN or $CHCl_3$ in 2 replicates in a quartz cuvette, with 1 cm optical path length. The area under the absorption curve for the known dye concentrations was compared to that of the MIP and dNIP particles in the respective solvents, to determine the amount of dye incorporated.

17. Fluorescence titration spectra of MIPa@SiO_2 with competing analytes in $CHCl_3$

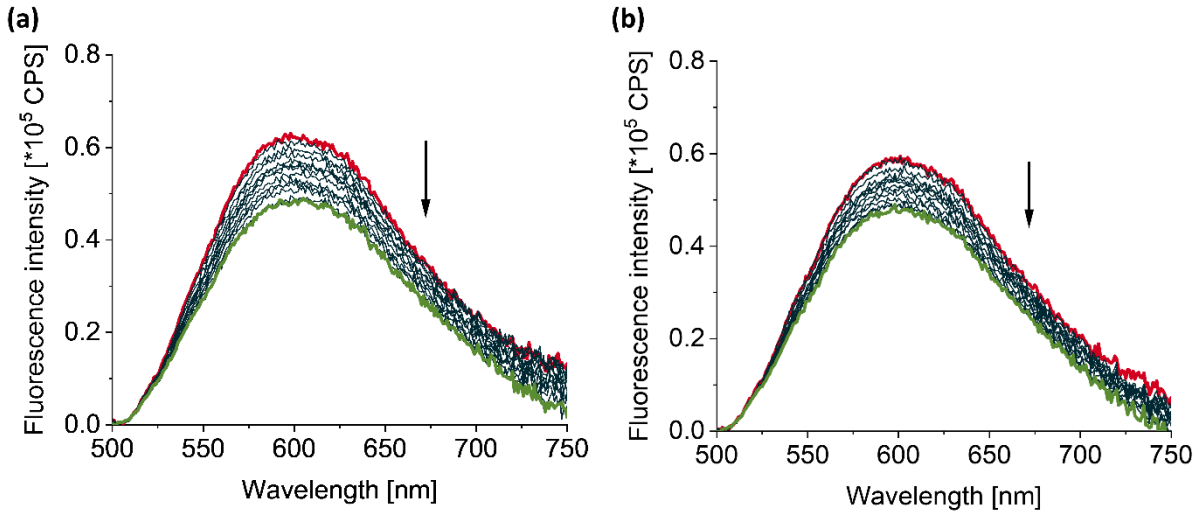

Figure S22. Fluorescence titration spectra (λ_{ex} = 474 nm), following the titration of **MIPa@SiO_2** in $CHCl_3$ with up to 200 μM of (**a**) 2,4-D-TBA and (**b**) dicamba-TBA. The red line shows the spectrum of **MIPa@SiO_2** in $CHCl_3$, while the green line shows the spectrum of **MIPa@SiO_2** after the addition of 200 μM of the corresponding template in $CHCl_3$.

18. Fluorescence titration spectra of MIPb@SiO$_2$ with competing analytes in MeCN

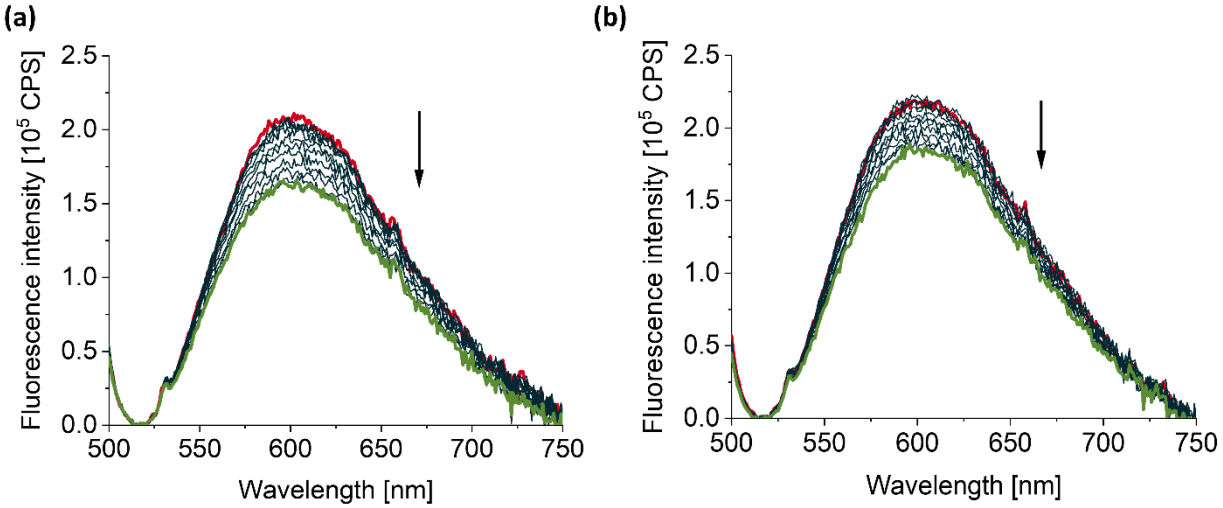

Figure S23. Fluorescence titration spectra (λ_{ex} = 483.5 nm) following titration of **MIPb@SiO$_2$** in MeCN with up to 200 μM of (**a**) 2,4-D-TBA and (**b**) dicamba-TBA. The red line is spectrum of **MIPb@SiO$_2$** in MeCN, while the green line shows the spectrum of **MIPb@SiO$_2$** after the addition of 200 μM of the corresponding template in MeCN.

19. Determination of LOB and LOD of MIPa@SiO$_2$ and MIPb@SiO$_2$

The parameters limit of blank (LOB) and limit of detection (LOD) describe the smallest concentration of a sample that can be reliably measured by an analytical procedure [3]. LOB is defined as the highest putative analyte concentration expected to be found when replicates of a blank sample in the absence of the analyte are measured. LOD is defined as the lowest analyte concentration likely to be reliably distinguished from the LOB and at which detection is feasible.

The absolute values of the fluorescence emission data at 593 nm (for **MIPa@SiO$_2$**) and 600 nm (for **MIPb@SiO$_2$**), following titration with increasing amounts of corresponding template (GPS-TBA in $CHCl_3$ or MeCN respectively), were fitted using a logistic function (Figure S15a and b). From the fitting equation, the concentration corresponding to the fluorescence response of three blank measurements was used to determine the limit of blank (LOB). Three repeat measurements of the lowest concentration of GPS-TBA used (0.50 μM for **MIPa@SiO$_2$** in $CHCl_3$ and 7.44 μM for **MIPb@SiO$_2$** in MeCN) were employed to determine the limit of detection (LOD). The LOB and LOD were calculated, as below [4]:

$$\boldsymbol{LOB = \bar{x}^0 + 1.645SD^{LOB}}$$

where $\boldsymbol{\bar{x}^0}$ is the concentration corresponding to the average response of 3 blank measurements (MIP particles without analyte) and $\boldsymbol{SD^{LOB}}$ is the standard deviation of these measurements:

$$\boldsymbol{LOD = LOB + 1.645SD^{LOD}}$$

where $\boldsymbol{SD^{LOD}}$ is the standard deviation of 3 measurements of the lowest concentration of analyte used.

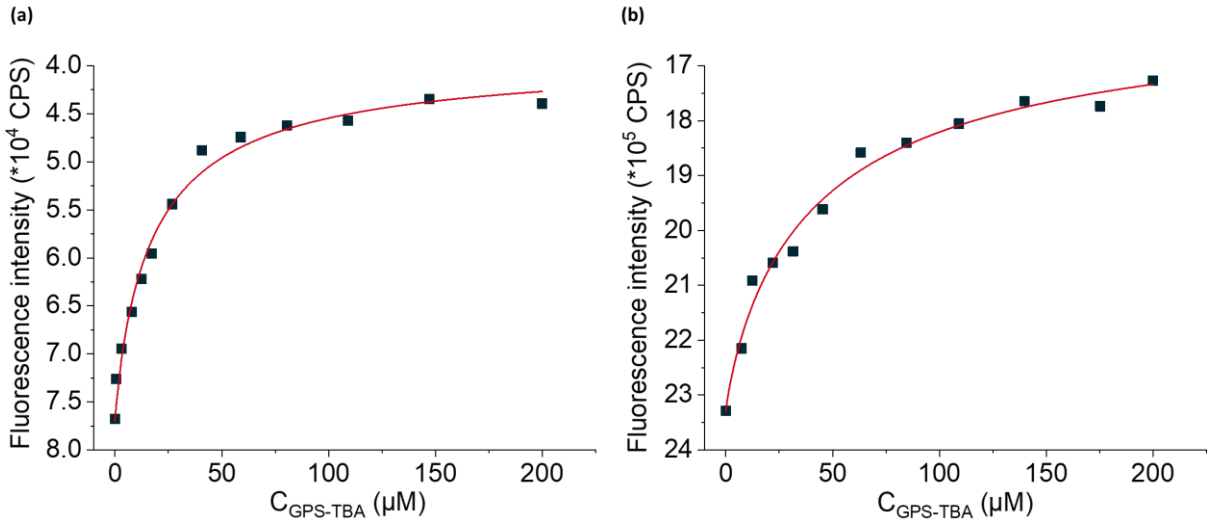

Figure S24. Logistic curve fitting using fluorescence emission intensity (**a**) at 593 nm for **MIPa@SiO₂** in $CHCl_3$ (λ_{ex} = 474 nm) and (**b**) at 600 nm for **MIPb@SiO₂** in MeCN (λ_{ex} = 483.5 nm). Here, 2 mL of 1 mg mL^{-1} suspensions of particles in the respective solvents were used.

20. Kinetics of binding for MIPa@SiO₂ and MIPb@SiO₂

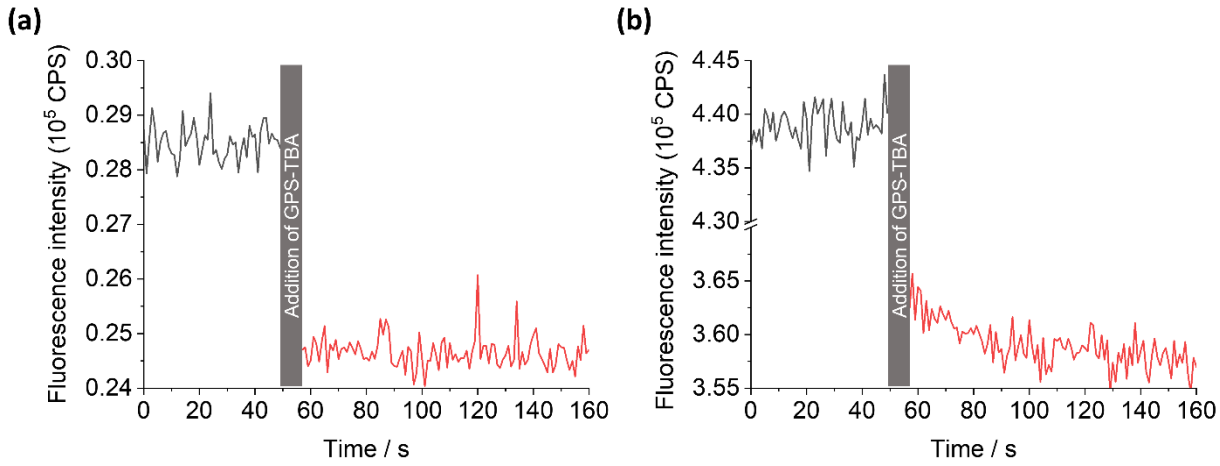

Figure S25. Kinetics of the interaction of 2 mL of 1 mg mL^{-1} (**a**) **MIPa@SiO₂** in $CHCl_3$ and (**b**) **MIPb@SiO₂** in MeCN after addition of 130 μM GPS-TBA, respectively, to the particle suspensions. The suspensions were mixed for 30 seconds for equilibration, after which the template solution was added and mixing continued. Similar results were expected for the dNIP particles, due to comparable shell thickness in the respective solvents. The signal decrease upon the addition of the template was virtually instantaneous in the case of $CHCl_3$, while in MeCN, it took ca. 30 s before equilibrium was reached. This can be explained by the longer diffusion times due to the thicker MIP shells that were formed when MeCN was used as a porogen during the synthesis. Kinetics were recorded at λ_{ex} = 474 nm and λ_{em} = 593 nm in $CHCl_3$, and λ_{ex} = 483 nm and λ_{em} = 600 nm in MeCN.

21. Uncertainty budget calculations

Because of the multiplicative and quotient forms of the respective equations and because correlations between the quantities are assumed to be negligible, the summation of the squares of the relative uncertainties was performed [5,6].

i. Weighing of ca. 2.0 mg of particles (balance, Mettler Toledo 1 ± 0.01 mg); ${}_{rel}^{w}u$= 0.5%

ii. Dissolution of particles in 2 mL solvent (Eppendorf Reference pipette ± 0.036 mL); ${}_{rel}^{d}u$= 1.8%

iii. Transfer of 2 mL particle suspension to cuvette (Eppendorf Reference pipette ± 0.008 mL); 2*${}_{rel}^{d2}u$= 2*0.8%; contribution from cell length (± 0.01 mm); ${}_{rel}^{L}u$=0.1%

iv. Addition of template solution to particle suspension during titrations (Eppendorf Reference pipettes); ${}_{rel}^{t}u$=1.0 – 2.2%

v. Relative uncertainty of emission; ${}_{rel}^{e}u$ = 0.6%

vi. Repetition of measurements; ${}_{rel}^{r}u$= 0.01 – 3.6%

Total relative error: $\sqrt{({}_{rel}^{w}u^2 + {}_{rel}^{d}u^2 + 2 * {}_{rel}^{d2}u^2 + {}_{rel}^{L}u^2 + {}_{rel}^{t}u^2 + {}_{rel}^{r}u^2)}$ = 2.3 – 5.1%

References

1. Wan, W.; Descalzo, A.B.; Shinde, S.; Weißhoff, H.; Orellana, G.; Sellergren, B.; Rurack, K. Ratiometric Fluorescence Detection of Phosphorylated Amino Acids Through Excited-State Proton Transfer by Using Molecularly Imprinted Polymer (MIP) Recognition Nanolayers. *Chem. Eur. J.* **2017**, *23*, 15974-15983, doi:10.1002/chem.201703041.
2. Brynn Hibbert, D.; Thordarson, P. The death of the Job plot, transparency, open science and online tools, uncertainty estimation methods and other developments in supramolecular chemistry data analysis. *Chem. Commun.* **2016**, *52*, 12792-12805, doi:10.1039/C6CC03888C.
3. Rurack, K.; Radeglia, R. Transition Metal Ion Complexes of 2,2′-Bipyridyl-3,3′-diol and 2,2′-Bipyridyl-3-ol: Spectroscopic Properties and Solvent-Dependent Binding Modes. *Eur. J. Inorg. Chem.* **2000**, *2000*, 2271-2282, doi:10.1002/1099-0682(200010)2000:10<2271::AID-EJIC2271>3.0.CO;2-3.
4. Armbruster, D.A.; Pry, T. Limit of blank, limit of detection and limit of quantitation. *Clin. Biochem. Rev.* **2008**, *29 Suppl 1*, S49-S52.
5. *Evaluation of measurement data — Guide to the expression of uncertainty in measurement*; JCGM 100:2008; Joint Committee for Guides in Metrology (JCGM): 2008; p 134, Availabe online: https://www.bipm.org/documents/20126/2071204/JCGM_100_2008_E.pdf/cb0ef43f-baa5-11cf-3f85-4dcd86f77bd6 (accessed on 25.10.2021).
6. Rurack, K.; Spieles, M. Fluorescence Quantum Yields of a Series of Red and Near-Infrared Dyes Emitting at 600−1000 nm. *Anal. Chem.* **2011**, *83*, 1232-1242, doi:10.1021/ac101329h.